ISSN 1063-7737, Astronomy Letters, 2017, Vol. 43, No. 9, pp. 614–623. © Pleiades Publishing, Inc., 2017.
Original Russian Text © P.A. Gritsyk, B.V. Somov, 2017, published in Pis'ma v Astronomicheskii Zhurnal, 2017, Vol. 43, No. 9, pp. 676–686.

Electron Acceleration in Solar-Flare Magnetic Traps: Model Properties and Their Observational Confirmations

P. A. Gritsyk* and B. V. Somov**

Sternberg Astronomical Institute, Moscow State University, Universitetskii pr. 13, Moscow, 119992 Russia

Received March 3, 2017

Abstract—Using an analytical solution of the kinetic equation, we have investigated the model properties of the coronal and chromospheric hard X-ray sources in the limb flare of July 19, 2012. We calculated the emission spectrum at the flare loop footpoints in the thick-target approximation with a reverse current and showed it to be consistent with the observed one. The spectrum of the coronal source located above the flare loop was calculated in the thin-target approximation. In this case, the slope of the hard X-ray spectrum is reproduced very accurately, but the intensity of the coronal emission is lower than the observed one by several times. Previously, we showed that this contradiction is completely removed if the additional (relative to the primary acceleration in the reconnecting current layer) electron acceleration in the coronal magnetic trap that contracts in the transverse direction and decreases in length during the impulsive flare phase is taken into account. In this paper we study in detail this effect in the context of a more realistic flare scenario, where a whole ensemble of traps existed in the hard X-ray burst time, each of which was at different stages of its evolution: formation, collapse, destruction. Our results point not only to the existence of first-order Fermi acceleration and betatron electron heating in solar flares but also to their high efficiency. Highly accurate observations of a specific flare are used as an example to show that the previously predicted theoretical features of the model find convincing confirmations.

DOI: 10.1134/S1063773717090031

Keywords: *Sun, magnetic fields, Fermi acceleration, betatron heating, solar flares, magnetic trap.*

1. INTRODUCTION

The acceleration of charged particles to high energies remains a topical problem of modern astrophysics as applied to phenomena different in their scales and nature: the gravitational collapse of stars and other astronomical objects (Becker 2009; Fleishman and Toptygin 2013), for example, protostellar clouds with a frozen-in magnetic field (Balogh et al. 2013), cosmic rays (Dorman 2009; Shalchi 2009; Miroshnichenko 2015), and solar flares. The latter are of particular interest for studying the physical particle acceleration mechanisms, because they can be investigated most comprehensively with high spatial, temporal, and spectral resolutions. At present, the achieved accuracy of electromagnetic radiation detectors onboard spacecraft is so high (Lin et al. 2002; Lemen et al. 2012; Christe et al. 2016; Hudson 2016) that the observational data allow us to reconstruct a complete picture of particle acceleration and propagation in the solar atmosphere and, thus, to check whether the existing model assumptions are correct.

*E-mail: pgritsyk@gmail.com
**E-mail: somov.boris@gmail.com

The overall picture and scenario of a solar flare may be considered without exaggeration to have been well studied (Somov 2012, 2013; Krucker et al. 2008; Zharkova et al. 2011; Emslie et al. 2012). Magnetic reconnection plays a decisive role in this manifestation of solar activity. Figure 1 schematically shows a two-dimensional picture of magnetic reconnection near the null point (Somov 2013) located in the corona. The plasma flows near this point are characterized by vectors $\mathbf{v}_0$ for the inflow velocity and $\mathbf{v}_1$ for the outflow velocity. The half of the reconnected flux directed downward is shown.

The reconnected magnetic field lines move from the layer together with a "super-hot" (an electron temperature $T_e \gtrsim 30$ MK), predominantly collisionless plasma toward the "magnetic obstacle," a region with a stronger magnetic field. It is painted gray in Fig. 1. The top of each magnetic loop formed upon reconnection moves together with the plasma with velocity $\mathbf{v}_1$ from the corona (Cor) toward the chromosphere (Ch). The loop footpoints are connected with the magnetic field sources, sunspots N and S on the photosphere (Ph). The dashed line in Fig. 1 indicates the shock wave (SW) possible in this scenario that separates the "hot" and "cold" plasmas.

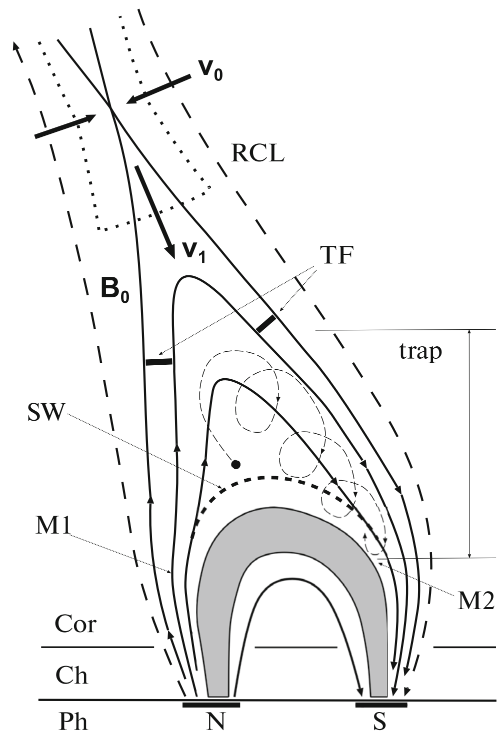

Fig. 1. The coronal magnetic trap (trap) between the turbulent front (TF) and the magnetic mirrors ($M1$, $M2$). The dashed spiral indicates the trajectory of a trapped electron. SW is the shock wave separating the hot and cold plasmas. RCL is the high-temperature reconnecting current layer, the source of primarily accelerated electrons.

At slow magnetic reconnection and a low coronal plasma density the shock wave does not necessarily emerge (Somov 2013).

The electrons and ions are pre-accelerated by the electric field in the reconnecting current layer (RCL in Fig. 1). After this first step in the acceleration process, they end up in the coronal magnetic trap (trap in Fig. 1), whose length and cross-sectional size (thickness) decrease rapidly (Somov and Kosugi 1997). In such a "collapsing" trap the captured particles are reflected from the shock wave or from the magnetic "mirrors" $M1$ and $M2$ in Fig. 1. Inside the collapsing trap the charged particles acquire an additional acceleration through the first-order Fermi mechanism and betatron heating. Such an increase in particle energy is of fundamental importance for the proper interpretation of observations, because in many flares allowance for the primary acceleration in the reconnecting current layer turns out to be insufficient (see, e.g., Section 3.3.2 in Krucker et al. (2008)). Such a picture was called double step acceleration in Somov and Kosugi (1997) and has not yet been confirmed by convincing observations of flares, remaining predominantly a theoretical prediction.

The July 19, 2012 flare was observed at the solar limb by the RHESSI, GOES, and SDO spacecraft (Liu 2013) with a high accuracy, making it suitable for investigating the magnitude and efficiency of the possible additional electron acceleration in the corona. The data on the spectrum, locations, and spatial scales of the coronal and chromospheric hard X-ray sources are described in detail in Krucker and Battaglia (2014) and Krucker et al. (2015).

We calculated the energy flux density of the electrons accelerated in the reconnecting current layer (RCL) or, more precisely, the fast electrons escaping from the current layer through the turbulent front (TF) in schematic Fig. 1 within the framework of a self-consistent thick-target model with a reverse current (Diakonov and Somov 1988; Litvinenko and Somov 1991; Gritsyk and Somov 2011). We applied the formalism of the thin-target model described in Somov and Syrovatskii (1976) to calculate the intensity of the coronal hard X-ray source. To explain the observed emission simultaneously in the chromosphere and the corona, we supplemented the models mentioned above (Gritsyk and Somov 2016) by the model of a collapsing magnetic trap (Somov and Kosugi 1997).

The goal of this paper is to investigate the double step electron acceleration and the role of coronal traps in solar flares based on data from present-day space experiments. As a good example, we chose the limb flare of July 19, 2012, for which highly accurate observations in various ranges of the electromagnetic spectrum are available. Our attention is focused on the secondary particle acceleration in collapsing magnetic traps. In contrast to previous publications, we demonstrate precisely how the trap contracts and its length decreases, which of the acceleration mechanisms prevails, what energy the electrons are accelerated to, and how their spectrum changes. For the first time we have shown a convincing observational proof of not only the existence of first-order Fermi acceleration and betatron electron heating in solar flares but also their high efficiency.

The paper is structured as follows. Section 2 provides observational data for the flare. Sections 3 and 4 are devoted to a theoretical consideration of the electron acceleration in collapsing magnetic traps, while Section 5 presents the flare modeling results. In Conclusions we formulate our conclusions and discuss the prospects for developing the subject.

2. MULTI-WAVELENGTH OBSERVATIONS OF THE FLARE

The $M7.7$ flare was observed on July 19, 2012, starting at 05:15 UT, with the RHESSI, GOES, SDO, NoRP, and NoRH instrumentation. The

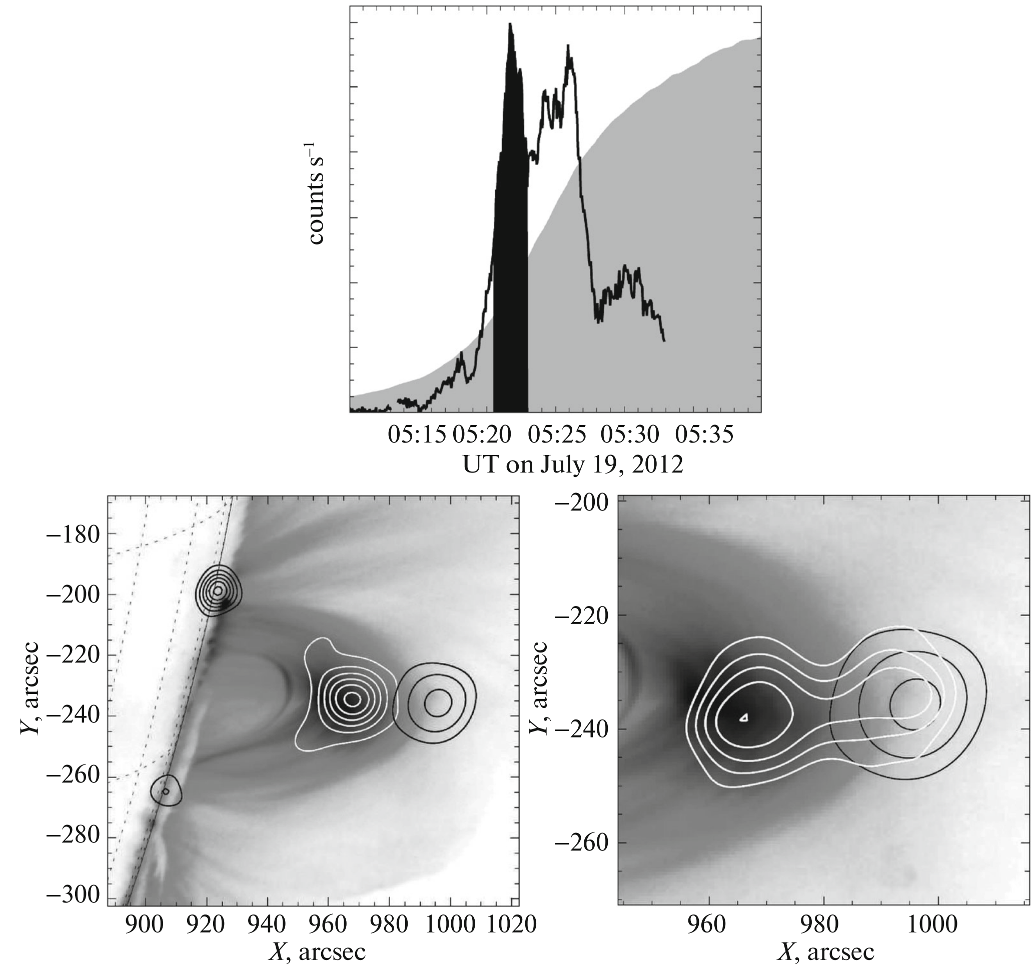

Fig. 2. Results of the observations of the July 19, 2012 flare. The upper panel shows the time profile of the hard X-ray emission from the entire flare (black line) based on RHESSI data in the range 30–80 keV. The gray background indicates the profile of the soft X-ray emission in the range 3–25 keV from GOES data. The lower panel shows the images at a wavelength of 193 Å obtained onboard SDO with the ultraviolet AIA telescope. The flare loop with the coronal and chromospheric sources is presented in the image on the left; the coronal source is on the right. The black contours indicate the hard X-ray levels from RHESSI data in the range 30–80 keV. The white contours indicate the soft X-ray levels: the ranges 6–8 and 16–18 keV are on the left and the right, respectively.

unprecedented accuracy of modern multi-wavelength detectors and the flare location at the solar limb allowed the flare loops to be simultaneously observed in the corona and the chromosphere with high temporal, spatial, and spectral resolutions (Liu et al. 2013; Liu 2013; Krucker and Battaglia 2014; Krucker et al. 2015).

Let us discuss in more detail the observed picture of the flare (Fig. 2). One coronal and two chromospheric sources were observed in hard X-rays. The southern chromospheric source is very faint, because it is partially behind the limb. In this paper we consider the northern chromospheric emission source using the approximation of the thick-target model with a reverse current. We will choose the energy flux density transferred by the flare-accelerated electrons in such a way that the emission spectrum corresponds to the experimental data. The RHESSI observations are presented in Krucker and Battaglia (2014) in the form of the addition of individual measurements in the time interval shown in Fig. 2 with the center at the first maximum of the hard X-ray burst (05:21:45 UT).

This time interval ($\sim$150 s) corresponds to the part of the impulsive flare phase when the electron acceleration was most efficient, while the intensity of hard X-ray bremsstrahlung was maximal. The total duration of the impulsive phase is much longer ($\sim$0.5 h; see, e.g., Liu 2013). This allows us to make the assumption about comparatively slow magnetic reconnection in this flare and, as a consequence, about the absence of a shock wave (SW) in it (see Fig. 1). The coronal hard X-ray source presented in Fig. 2 was above the flare loop. We chose the thin-target approximation for its description. The formalism of the thin-target model we use was taken from Somov and Syrovatskii (1976).

Let us list the main parameters accessible from observations that will be used for our calculations in the kinetic flare model. The coronal hard X-ray source is in the immediate vicinity of the electron acceleration region, a high-temperature reconnecting current layer (RCL in Fig. 1) and, according to the estimates by Krucker and Battaglia (2014), has an angular size of 15″. The lower boundary of the energy spectrum for the flare-accelerated electrons is $\mathcal{E}_{\min} \approx 15$ keV. As a rule, this quantity is estimated with a large error due to the superposition of thermal and nonthermal injection spectra characteristic for any flare (Somov and Syrovatskii 1976). This fact introduces inaccuracies in determining the intensity of the hard X-ray emission but hardly affects the estimate of the most important observed parameter in the spectrum, its slope.

The upper boundary of the spectrum is not known with certainty. We will arbitrarily assume it to be $\mathcal{E}_{\max} = 120$ keV. This does not disturb the physical picture of the process, because the high-energy electrons hardly experience any Coulomb collisions and the action of the reverse-current electric field and contribute insignificantly to the intensity of the observed X-ray emission. Nevertheless, these electrons (Holt and Ramaty 1969) make a significant contribution to the high-frequency part of the gyrosynchrotron radio spectrum, which is not considered in this paper.

We will give here some important estimates of various parameters for the July 19, 2012 flare from Krucker and Battaglia (2014). The temperature of the "cold" target plasma behind the turbulent front (TF in Fig. 1) is high, $T_2 \approx 21$ MK. The temperature of the source of accelerated electrons, i.e., the super-hot plasma near the reconnection region, is not known from observations and is taken to be $T_1 \approx 100$ MK, i.e., it is estimated in order of magnitude based on the theory of super-hot turbulent current layers (Ch. 8 in Somov 2013). The plasma density in the region where the coronal source is located is $n_2 \approx 3 \times 10^9$ cm^{-3} (see Fig. 8.8 in Somov 2013). The coronal source has a spectral slope $\varphi = 4.6 \pm 0.2$ with a flux of 0.1 photons cm^{-2} keV^{-1} at a photon energy of 50 keV, while the chromospheric one has $\varphi = 3.0 \pm 0.2$ with a flux of 1 photon cm^{-2} keV^{-1}.

As has been noted above, the observational characteristics (primarily the spectral ones) of the hard X-ray flare emission presented in this section are the result of the addition of individual observations in the interval of the first X-ray maximum, $\sim$150 s. In this time several collapsing traps are created and destroyed in the corona (trap in Fig. 1), with the characteristic lifetime of each of them being $\sim$10 s (Somov and Kosugi 1997) or, minus their formation time, $\sim$5 s. Thus, the intensities of the coronal and chromospheric sources change noticeably in the time of the addition of X-ray images. Therefore, when interpreting the observations, by the flare model we will mean the averaging over all the particular models describing the flare at a given time. To estimate the electron acceleration efficiency in such an averaged collapsing trap, we need its mirror ratio b_m (Bogachev and Somov 2007), which is not known from observations. We will consider it to be a free parameter and choose it in such a way that the intensity of the X-ray emission in the corona corresponds to the observed one. In addition, estimates of the contraction parameters for the averaged trap allow us to make assumptions about the role of Fermi acceleration and betatron heating in the flare under consideration. These simplifications create some freedom in interpreting the observations but allow the electron acceleration in the trap to be understood qualitatively.

Depending on the mirror ratio b_m, the trap can confine up to 99% of the particles (Bogachev and Somov 2005) that precipitated from the source and, as a consequence, can reduce significantly the emission intensity in the chromosphere at the time of its existence. We found one example of such a situation at the very beginning of the impulsive phase of the July 19, 2012 flare. It can be seen from Fig. 3, where three panels with the RHESSI images of the hard X-ray sources at various times are presented. The left and central panels refer to the beginning of the impulsive phase of the flare (see Fig. 2), whose development in time is shown on the right panel. These observations can point to the existence of coronal traps and can confirm our views of the physics of the processes in them.

3. A COLLAPSING MAGNETIC TRAP

Present-day space experiments (Dennis et al. 2011; Hudson 2016) show that the particle acceleration efficiency in the corona is very high. The main mechanism for the conversion of the flare magnetic energy (Aschwanden et al. 2016) into the kinetic energy of charged particles is the electric field that emerges in the corona during magnetic reconnection (Somov 2012, 2013; Zharkova et al. 2011). In many flares allowance for this primary acceleration turns out to be insufficient for the interpretation of observations in the corona and the chromosphere. Somov and Kosugi (1997) offered a description of the electron acceleration in a flare where the particles acquire an additional energy inside the coronal magnetic trap as it contracts in the longitudinal and transverse directions. The particle acceleration in this case is attributable to two mechanisms (Somov and

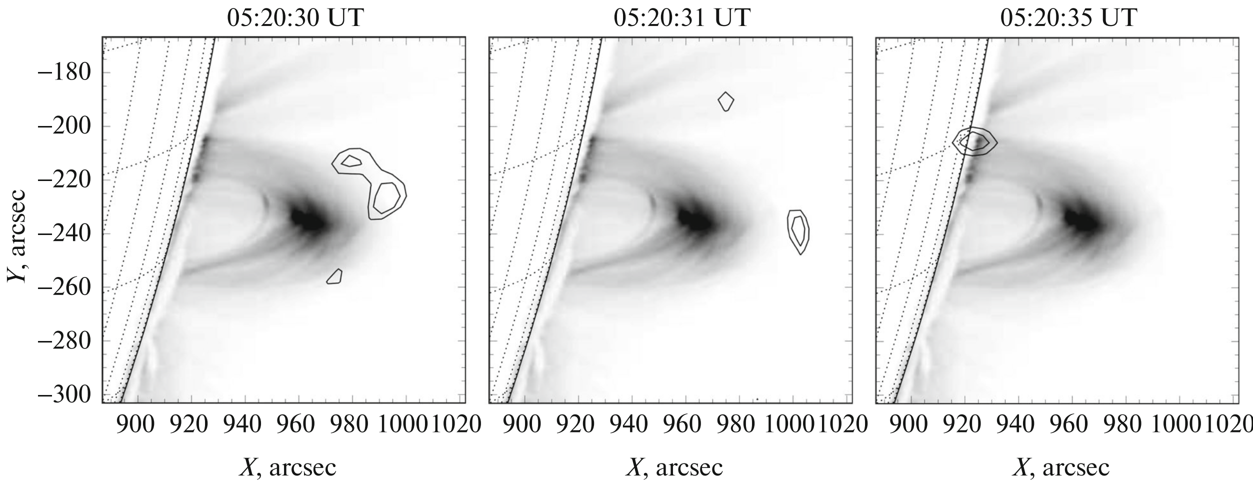

Fig. 3. Results of the observations of the July 19, 2012 flare. The background of each panel is the image of the flare loop at a wavelength of 193 Å obtained onboard SDO with the ultraviolet AIA telescope. The black contours indicate the hard X-ray levels from RHESSI data in the range 30–80 keV. The time of observations is shown above each panel.

Bogachev 2003): the first-order Fermi acceleration and the betatron acceleration for the longitudinal and transverse contraction, respectively.

The physics of these processes is easy to show. If the period of the motion of particles between the magnetic mirrors ($M1$ and $M2$ in Fig. 1) is much shorter than the trap lifetime, while the particle Larmor radius is much smaller than the length scales of the change in magnetic field and if other conditions of the adiabatic approximations are fulfilled (see, e.g., Somov 2013; Bogachev and Somov 2005), then the longitudinal,

$$p_{||}L = p_{||0}L_0 = \text{const} \quad (1)$$

and transverse,

$$p_{\perp}^2/B = p_{\perp 0}^2/B_0 = \text{const}, \quad (2)$$

adiabatic invariants are conserved as the trap contracts, where $p_{||}$ and $p_{\perp}$ are the longitudinal and transverse particle momenta, L_0 and B_0 are the initial values of the trap length and the magnetic field strength inside the trap, L and B are the current values of the trap length and the magnetic field strength inside the trap. Equations (1) and (2) can be rewritten in dimensionless parameters $b = B/B_0$ and $l = L/L_0$:

$$p_{||} = \frac{p_{||0}}{l}, \quad (3)$$

$$p_{\perp} = p_{\perp 0}\sqrt{b}. \quad (4)$$

Equation (3) characterizes the first-order Fermi acceleration, when the longitudinal particle momentum increases and the transverse one remains constant as the trap length l decreases with time. In contrast, the betatron acceleration increases the transverse momentum and does not change the longitudinal one (4). Of course, both mechanisms can operate in solar flares.

Equations (3) and (4) characterize the change in the velocity and, consequently, kinetic energy of a particle captured into a collapsing magnetic trap. Let us determine the change in its pitch angle under the combined action of the two acceleration mechanisms. For this purpose, we will write the expression

$$\tan\theta = \frac{p_{\perp}}{p_{||}} = l\sqrt{b}\left(\frac{p_{\perp 0}}{p_{||0}}\right) = l\sqrt{b}\tan\theta_0, \quad (5)$$

where θ_0 and θ are the initial and current particle pitch angles, respectively. It can be seen from Eq. (5) that at $l\sqrt{b} = 1$ the trap does not change the particle pitch angle distribution. If $l\sqrt{b} < 1$, then the particle pitch angle becomes smaller as the trap contracts, while the first-order Fermi mechanism is dominant. In contrast, at $l\sqrt{b} > 1$ the pitch angle increases and the betatron acceleration is dominant. The particles are in the trap and are accelerated until they fall into the loss cone. The tangent of the pitch angle at this time is defined by the expression (Bogachev and Somov 2005)

$$\tan\theta_{\text{esc}} = \frac{1}{\sqrt{b_m/b - 1}}. \quad (6)$$

The particles with a pitch angle $\theta \leq \theta_{\text{esc}}$ pass through the mirrors unimpeded and precipitate into the chromosphere, where they lose their energy through Coulomb collisions and generate hard X-ray bursts. As has been noted in Section 2, there are few such particles. In other words, situations where there is no emission from the chromosphere in the presence of a source in the corona are possible, which we detected using the observations of the July 19, 2012 flare as an example (see Fig. 3). Nevertheless, in many flares the observed picture is much more complex and varied due to the superposition of traps at different phases of evolution on one another in time. As has been noted, in this paper we will consider the averaged flare parameters.

The kinetic model describing the X-ray sources is discussed in the next section. Here, to conclude the general consideration of a coronal magnetic trap, we will note an important fact detailed in Somov and Bogachev (2003) and Bogachev and Somov (2005). The authors proved that the transverse trap contraction or expansion (betatron heating) did not affect the energy acquired by a particle during its acceleration. This is related to a growth of the loss cone and, as a consequence, an earlier particle escape from the trap, which, nevertheless, is exactly compensated for by the faster energy accumulation. This peculiarity does not imply the absence of observational manifestations of the betatron acceleration; after all the trap confines the particles better. The density of trapped electrons and their total kinetic energy reach values that exceed (Bogachev and Somov 2005) the maximum possible values of these quantities in a trap with the dominant Fermi acceleration by several times. As a consequence, one might expect much higher intensities of the hard X-ray emission generated by the trapped electrons as they collide with background coronal plasma particles. In other words, in flares where a bright coronal (at the loop top) hard X-ray source is observed, the existence of betatron electron heating and its high efficiency can be assumed. The July 19, 2012 flare being considered here is a dramatic example of such an event.

4. THE SPECTRUM OF ELECTRONS AND THEIR BREMSSTRAHLUNG

At present, the assertion that the hard X-ray bursts observed near the Earth during solar flares are associated with the bremsstrahlung of accelerated electrons propagating in the solar corona and chromosphere is deemed universally accepted (Hudson and Ryan 1995; Somov 2000; Aschwanden 2002; Somov 2013). Various kinetic models are used to describe this process. In this section of the paper we give a brief description of the most detailed analytical flare model that allows both the coronal hard X-ray source (in the approximation of the thin-target model supplemented by the model of a collapsing magnetic trap) and the chromospheric source (in the approximation of the thick-target model with a reverse current) to be modeled with a high accuracy.

It has been noted previously that the coronal part of the flare (see Fig. 1) can be divided into two parts: the electron acceleration region near the reconnecting current layer (RCL) with temperature T_1 and the region of a colder plasma with temperature T_2. A thin turbulent front (TF) is formed between these regions, below which we solve the kinetic problem of the propagation of accelerated electrons. The long (see Section 2) impulsive phase of the July 19, 2012 flare suggests slow magnetic reconnection. Therefore, we will assume the absence of a shock wave (SW in Fig. 1) in the time interval under consideration.

The most powerful X-ray source is the chromospheric flare loop footpoint. A theoretical description of such a source was offered in the first self-consistent analytical models (Syrovatskii and Shmeleva 1972; Brown 1971), whose accuracy allowed the space observations of that time to be properly explained. The models with a reverse current (Diakonov and Somov 1988; Litvinenko and Somov 1991) became a natural development of the kinetic theory of solar flares and were successfully applied to the description of new highly accurate observations (Gritsyk and Somov 2014, 2016). Let us consider one of these models.

The electron distribution function in the source, in a super-hot turbulent reconnecting current layer, consists of two parts: the thermal and nonthermal ones. The former is usually taken in a Maxwellian form; the latter is taken in the form of a power law. We will consider the fast electrons of a nonthermal nature. Therefore, as the boundary one (at the boundary TF) we will take only the part of the distribution function of electrons in their source in the form of a power law:

$$f_{\mathbf{v}}(v,\theta,0) = K_0 v^{-\gamma_{\mathbf{v}}} \Theta(v - v_{\min})\Theta(v_{\max} - v), \quad (7)$$

where v is the magnitude of the electron velocity, $v_{\min}$ and $v_{\max}$ are its minimum and maximum values, the theta function $\Theta(x) = 1$ at $x \geq 0$ and $\Theta(x) = 0$ at $x < 0$. Here and below, the index $\mathbf{v}$ indicates that $f_{\mathbf{v}}$ is the particle velocity vector distribution function. The constant K_0 is determined from the condition for the normalization of the distribution function to the energy flux density being transferred by the flare-accelerated electrons:

$$F = \int f_{\mathbf{v}}(v,\theta) v \cos\theta \frac{m_e v^2}{2} d^3\mathbf{v} \ \mathrm{erg\,cm^{-2}\,s^{-1}}, \quad (8)$$

where m_e is the electron mass. When modeling a flare, the parameter (8) is chosen so that the calculated intensity of the X-ray emission from the chromospheric source corresponds to the observed one.

A key feature of this thick-target model is allowance for the reverse current that affects significantly the propagation of electrons in the flare (Gritsyk and Somov 2014). The forward-flying accelerated electrons produce an electric current that will be called the direct one. Given the sign of the electron charge, the direct current is directed toward the turbulent front (TF in Fig. 1). The reverse current is produced by the thermal electrons of the cold plasma inside the target moving under the action of the reverse-current electric field, which can be found from Ohm's law. A significant but justified assumption here is that the direct current is balanced by the reverse one. It implies that the very fast reverse-current generation (Van den Oord 1990) manages to balance the direct current in a time comparable to the period of plasma oscillations, which is much shorter than the time of Coulomb collisions under the conditions we consider.

We will describe the behavior of the distribution function of accelerated electrons in the target by the kinetic equation (see Section 4.5.2 in Somov 2012)

$$\upsilon \cos\theta \frac{\partial f_{\mathbf{v}}}{\partial r} - \frac{eE}{m_e}\cos\theta \frac{\partial f_{\mathbf{v}}}{\partial \upsilon} - \frac{eE}{m_e \upsilon}\sin^2\theta \frac{\partial f_{\mathbf{v}}}{\partial \cos\theta} = St_{\mathrm{L}}(f_{\mathbf{v}}), \quad (9)$$

where r is the penetration depth of particles into the target, e is the electron charge, and E is the reverse-current electric field strength. Here, we take into account the fact that on time scales of the order of the Coulomb collision time in the cold target plasma we may consider the injection of electrons as a stationary process and their distribution in the target as a steady-state one (the derivative $\partial/\partial t$ is zero). There is a linearized Landau collision integral on the right-hand side of the equation.

Gritsyk and Somov (2011) found an analytical solution of the kinetic equation (9) at a specified boundary condition (7). The solution unambiguously defines the evolution of the beam of accelerated particles in the target and allows the characteristics of the hard X-ray emission generated by them to be calculated.

For this purpose, we will use the well-known formulas (Elwert and Haug 1970) for the differential X-ray bremsstrahlung cross sections. The parameters needed to calculate the characteristics of the emission from the July 19, 2012 flare are presented in Section 2.

Here, we will note several important assumptions. When calculating the hard X-ray emission from accelerated electrons in specific solar flares, Syrovatskii and Shmeleva (1972) arbitrarily assumed the upper boundary of the electron energy spectrum to be infinitely large. This is quite justified. The slope is $\gamma_{\mathbf{v}} \gtrsim 2$ even for powerful flares with a very hard injection spectrum; therefore, the flux density estimates hardly change depending on the choice of an upper boundary for the spectrum (see also Gritsyk and Somov 2014).

Gritsyk and Somov (2016) showed that the solution of Eq. (9) describes well the distribution function at both small ($r \sim 0$, the thin-target approximation) and large ($r \to \infty$, the thick-target approximation with a reverse current) target thicknesses. Therefore, we will use it to calculate the intensity of the X-ray emission not only from the chromospheric source but also from the coronal one. However (see Section 3), it is impossible to properly estimate the intensity of the hard X-ray emission in the corona if the electron capture and acceleration in the collapsing magnetic trap are disregarded in the model of the coronal source (Somov and Kosugi 1997; Somov and Bogachev 2003). Bogachev and Somov (2007) showed that under the action of the betatron and Fermi accelerations the initially power-law electron injection spectrum calculated in the thin-target approximation remains the power-law one, while the coefficient K_0 increases according to the formula

$$K = K_0 \frac{\sqrt{1+(b_m - b)\,l^2}}{b\sqrt{b_m - b}} \times \int_0^{\sqrt{1-b/b_m}} \left[\frac{1 + x^2\left(bl^2 - 1\right)}{b}\right]^{-\gamma_{\mathcal{E}}} dx, \quad (10)$$

where $\gamma_{\mathcal{E}}$ is the slope of the energy spectrum for the accelerated electrons. This peculiarity of the particle acceleration is a significant observational manifestation indicative of an efficient particle acceleration in the coronal trap.

In the next section we discuss the kinetic modeling results for the July 19, 2012 flare. To conclude the current section, we will note yet another simplifying assumption. We will assume that the electron pitch angle distribution is isotropic at the boundary TF (Fig. 1). Of course, this assumption is rough, but quite justified, because even an initially nonisotropic electron distribution function is rapidly isotropized under the action of the reverse-current electric field and Coulomb collisions with background plasma particles (Litvinenko and Somov 1991).

5. MODELING RESULTS

The solid line in Fig. 4 represents the hard X-ray spectrum for the chromospheric source of the July 19, 2012 flare that was calculated in the thick-target model with a reverse current (see Section 5). To compare the models, the table gives the estimates obtained in the classical thick-target approximation, where the reverse current is disregarded.

It is clearly seen from Fig. 4 that the calculated X-ray spectrum in the chromosphere closely coincides with the observed one in both intensity and slope. For the convenience of understanding the table, note how the slopes of the electron injection spectra are related between themselves:

$$\gamma_{SS} = \gamma_{\mathcal{E}} - 1/2 = \gamma_{\mathbf{v}} - 1, \quad (11)$$

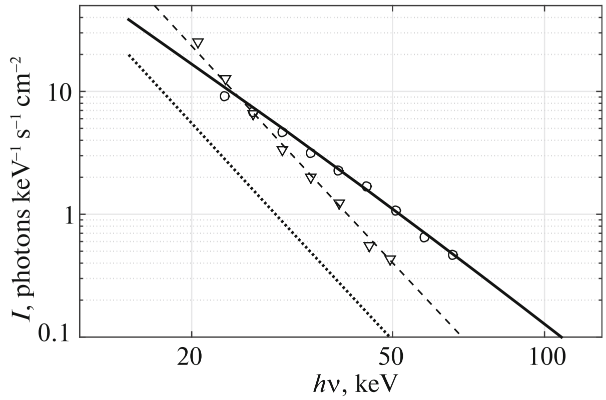

Fig. 4. Observed and calculated hard X-ray spectra for the July 19, 2012 solar flare. The results of modeling the chromospheric source are represented by the straight solid line; the observations are indicated by the circles. The results of modeling the coronal source without and with allowance for the electron acceleration in the collapsing magnetic trap are represented by the dotted and dashed straight lines, respectively; the observations are indicated by the triangles.

where γ_{SS} is the slope of the energy spectrum for the beam of accelerated electrons. The parameters of the electron beam n_b (particle density) and F (energy flux density) are given for the boundary TF (Fig. 1).

The spectrum of the coronal source calculated in the thin-target approximation (Somov and Syrovatskii 1976) is also presented in Fig. 4. Here, we will discuss the first important conclusion of this paper: it is fundamentally impossible to model the observed spectra of the coronal and chromospheric hard X-ray sources in terms of the classical flare model. Indeed (see the table), $\varphi_{\rm Cor} - \varphi_{\rm Ch} = 2$ always in the classical model, while according to the observations of the July 19, 2012 flare, $\varphi_{\rm Cor} - \varphi_{\rm Ch} \approx 1.6$. In the model with a reverse current the observed ratio of the slopes is naturally obtained for the flare parameters given in Section 2. In other words, the thick-target approximation with a reverse current not only accurately describes the X-ray spectrum of the chromospheric source but also allows the slope of the spectrum in the corona to be properly estimated. The intensity of the coronal source (the dotted line in Fig. 4), which is lower in the model than the observed one by a factor of $\approx$4.5, constitutes an exception. In our opinion, such a marked difference between the calculated and observed intensities, while the spectral slopes closely coincide, is a weighty argument for the idea of the existence of particle acceleration and its high efficiency in the collapsing magnetic trap formed by convergent magnetic field lines in the upper part of the flare loop (Fig. 1). Such an observational picture was predicted theoretically by Bogachev and Somov (2007), but in the absence of accurate space experiments it has had no convincing confirmation until now.

To determine the possible values for the longitudinal (l) and transverse (b) contraction coefficients of the coronal trap during the flare, we will use Eq. (10) by substituting $K/K_0 \approx 4.5$ into it. Let the mirror ratio unknown from observations be small, for example, $b_m = 3$. This assumption characterizes low-efficiency magnetic traps, because the energy accumulation in them is comparatively small. In traps with a larger mirror ratio b_m the energy accumulation will be not only larger but also faster.

Figure 5 presents the possible values for the parameters l and b at which $K/K_0 \approx 4.5$ at $b_m = 3$. Liu et al. (2013) provided estimates for the height of the flare loop top based on observational data in various spectral ranges, which hardly changed during the impulsive flare phase. Therefore, it can be assumed that the trap length also changed insignificantly and, consequently, the transverse contraction, i.e., the particle acceleration through betatron heating, dominated in the flare under consideration. A faster acceleration and precipitation into the chromosphere are charac-

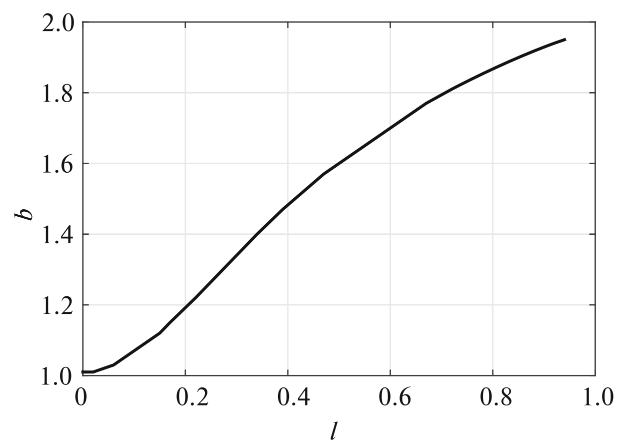

Fig. 5. Possible values for the longitudinal l and transverse b contraction parameters of the trap that provide a ratio of the coefficients $K/K_0 \approx 4.5$ at the mirror ratio $b_m = 3$.

Characteristics of the beam of accelerated electrons in the models with and without a reverse current

Model	$\gamma_{\mathbf{v}}$	$\gamma_{\mathcal{E}}$	γ_{SS}	n_b, cm^{-3}	F, erg cm^{-2} s^{-1}	$\varphi_{\rm Cor}$	$\varphi_{\rm Ch}$
Without reverse current	5.0	4.5	4.0	6.6×10^7	1.0×10^{10}	5.0 (4.6)	3.0 (3.0)
With reverse current	4.5	4.0	3.5	3.1×10^8	5.0×10^{10}	4.5 (4.6)	3.0 (3.0)

teristic for the particles captured into such traps (see Section 3), while the X-ray emission in the corona generated by them has a high intensity (the dashed line in Fig. 4).

All of the results presented in this section were obtained within the framework of analytical models. We interpreted the coronal source in the thin-target approximation supplemented by the model of a collapsing magnetic trap and the chromospheric source in the thick-target approximation with a reverse current. With a minimal set of parameters and model assumption we were able to model the results of space observations (see Section 2) for the July 19, 2012 solar flare with a high accuracy. To all appearances, in solar flares with powerful coronal hard X-ray sources the additional electron acceleration in the collapsing magnetic trap located in the corona plays a decisive role.

6. CONCLUSIONS

We considered a model for the limb flare of July 19, 2012, for which highly accurate satellite observations (primarily from the RHESSI spacecraft) are available. This flare was chosen for our modeling due to the presence of a bright coronal hard X-ray source (cf. Masuda 1994), which was observed synchronously with the sources located in the chromosphere near the flare loop footpoints. The flare model is based on the analytical methods proposed in earlier papers (Syrovatskii and Shmeleva 1972; Somov and Kosugi 1997; Litvinenko and Somov 1991; Somov and Bogachev 2003; Gritsyk and Somov 2014). The classical flare model based on the thick-target approximation was shown to be inapplicable for the description of solar flares with a coronal X-ray source, because it incorrectly predicts the slope of its spectrum. Recall that $\varphi_{\rm Cor} - \varphi_{\rm Ch} \approx 1.6$ for the July 19, 2012 flare, while in accordance with the classical model $\varphi_{\rm Cor} - \varphi_{\rm Ch} = 2$. This is an obvious confirmation that the reverse current needs to be taken into account even in comparatively small (in power) flares.

Our attention was focused on investigating the coronal hard X-ray source that, in our opinion, is attributable to the existence of collapsing magnetic traps produced by magnetic reconnection. One of the arguments for this are the results of observations at the beginning of the impulsive phase of the flare (Fig. 3) with the characteristic absence of a chromospheric source, which is presumably related to the existence of magnetic traps that efficiently confine the electrons and protons accelerated in the current layer. Such particles do not precipitate into the chromosphere and, as a consequence, do not create a chromospheric emission source. At the instant the trap ceases to confine them, an intense X-ray emission is observed at the flare loop footpoints. It is important to understand that a whole ensemble of coronal traps exists in the flare, each of which is at one of the evolutionary stages (formation, collapse, or destruction) with a characteristic lifetime $\sim$10 s. It is impossible to trace the development of each individual trap in the absence of instruments with sufficient spatial and temporal resolutions; therefore, in this paper we considered a trap with averaged contraction parameters. The results obtained in this approximation (Fig. 5) point to the predominant role of betatron heating in the particle acceleration in the trap during the July 19, 2012 solar flare.

Convincing arguments for the existence of coronal traps and their decisive role in the particle acceleration in solar flares constitute the main result of this paper. This result was obtained from general assumptions about the pattern of particle acceleration during solar flares, with the main one being the assumption about the existence of double step electron acceleration (Somov and Kosugi 1997), when the primarily accelerated particles in the reconnecting current layer acquire an additional acceleration, being captured into a contracting magnetic trap. The thin-target model predicts very accurately the slope of the X-ray spectrum in the corona and, being supplemented by the coronal trap, its intensity. The electron acceleration results from the action of two mechanisms: betatron heating and first-order Fermi acceleration. Owing to the existing and prospective space experiments (Grefenstette et al. 2016), one might expect new confirmations of our conclusions.

ACKNOWLEDGMENTS

We thank the referees for their useful remarks. This work was supported by the Russian Foundation for Basic Research (project no. 16-02-00585A).

REFERENCES

1. M. J. Aschwanden, *Particle Acceleration and Kinematics in Solar Flares* (Kluwer Academic, Dordrecht, 2002), p. 227.
2. M. J. Aschwanden, Astrophys. J. **832**, 27 (2016).
3. A. Balogh, A. Bykov, R. P. Lin, J. Raymond, and M. Scholer, *Particle Acceleration in Cosmic Plasmas* (Springer, New York, 2013), p. 640.
4. W. Becker, *Neutron Stars and Pulsars* (Springer, Berlin, Heidelberg, 2009), p. 697.
5. S. A. Bogachev and B. V. Somov, Astron. Lett. **31**, 537 (2005).
6. S. A. Bogachev and B. V. Somov, Astron. Lett. **33**, 54 (2007).
7. J. C. Brown, Solar Phys. **18**, 489 (1971).
8. S. Christe, L. Glesener, C. Buitrago-Casas, et al., J. Astron. Instrum. **5**, 625 (2016).
9. B. R. Dennis, A. G. Emslie, and H. S. Hudson, Space Sci. Rev. **159**, 3 (2011).
10. S. V. Diakonov and B. V. Somov, Solar Phys. **116**, 119 (1988).
11. L. Dorman, *Cosmic Rays in Magnetospheres of the Earth and Other Planets* (Springer Science, New York, 2009), p. 770.
12. G. Elwert and E. Haug, Solar Phys. **15**, 234 (1970).
13. A. G. Emslie, B. R. Dennis, R. P. Lin, and H. Hudson, *High-Energy Aspects of Solar Flares* (Springer, New York, 2012), p. 478.
14. G. D. Fleishman and I. N. Toptygin, *Cosmic Electrodynamics: Electrodynamics and Magnetic Hydrodynamics of Cosmic Plasmas* (Springer Science, New York, 2013), p. 712.
15. B. W. Grefenstette, L. Glesener, S. Krucker, H. Hudson, I. G. Hannah, D. M. Smith, J. K. Vogel, S. M. White, et al., Astrophys. J. **826**, 20 (2016).
16. P. A. Gritsyk and B. V. Somov, Mosc. Univ. Phys. Bull. **66**, 466 (2011).
17. P. A. Gritsyk and B. V. Somov, Astron. Lett. **40**, 499 (2014).
18. P. A. Gritsyk and B. V. Somov, Astron. Lett. **42**, 531 (2016).
19. S. S. Holt and R. Ramaty, Solar Phys. **8**, 119 (1969).
20. H. Hudson, Solar Phys. **291**, 1273 (2016).
21. H. Hudson and J. Ryan, Astrophys. J. **33**, 239 (1995).
22. S. Krucker and M. Battaglia, Astrophys. J. **780**, 107 (2014).
23. S. Krucker, M. Battaglia, P. J. Cargill, et al., Astron. Astrophys. Rev. **16**, 155 (2008).
24. S. Krucker, P. Saint-Hilaire, H. S. Hudson, M. Haberreiter, J. C. Martinez-Oliveros, M. D. Fivian, G. Hurford, L. Kleint, et al., Astrophys. J. **802**, 19 (2015).
25. J. R. Lemen, A. M. Title, D. J. Akin, P. F. Boerner, C. Chou, J. F. Drake, D. W. Duncan, C. G. Edwards, et al., Solar Phys. **275**, 17 (2012).
26. R. P. Lin, B. R. Dennis, G. J. Hurford, D. M. Smith, A. Zehnder, P. R. Harvey, D. W. Curtis, D. Pankow, et al., Solar Phys. **210**, 3 (2002).
27. Yu. E. Litvinenko and B. V. Somov, Solar Phys. **131**, 319 (1991).
28. R. Liu, Mon. Not. R. Astron. Soc. **434**, 1309 (2013).
29. W. Liu, O. Chen, and V. Petrosian, Astrophys. J. **767**, 168 (2013).
30. S. Masuda, T. Kosugi, H. Hara, S. Tsuneta, and Y. Ogawara, Nature **371**, 495 (1994).
31. L. I. Miroshnichenko, *Solar Cosmic Rays, Fundamentals and Applications,* 2nd ed. (Springer, Heidelberg, 2015).
32. G. H. J. van den Oord, Astron. Astrophys. **234**, 496 (1990).
33. A. Shalchi, *Nonlinear Cosmic Ray Diffusion Theory* (Springer, Berlin, Heidelberg, 2009), p. 199.
34. B. V. Somov, *Cosmic Plasma Physics* (Kluwer Academic, Dordrecht, 2000).
35. B. V. Somov, *Plasma Astrophysics. Part I: Fundamentals and Practice* (Springer Science, New York, 2012).
36. B. V. Somov, *Plasma Astrophysics, Part II: Reconnection and Flares* (Springer Science, New York, 2013), p. 504.
37. B. V. Somov and S. A. Bogachev, Astron. Lett. **29**, 621 (2003).
38. B. V. Somov and T. Kosugi, Astrophys. J. **485**, 859 (1997).
39. B. V. Somov and S. I. Syrovatskii, Sov. Phys. Usp. **19**, 813 (1976).
40. S. I. Syrovatskii and O. P. Shmeleva, Sov. Astron. **16**, 273 (1972).
41. V. V. Zharkova, K. Arzner, A. O. Benz, P. Browning, C. Dauphin, A. G. Emslie, L. Fletcher, E. P. Kontar, et al., Space Sci. Rev. **159**, 357 (2011).

Translated by V. Astakhov